Inorganic Chemistry

ARTICLE

pubs.acs.org/IC

Nature of Halide Binding to the Molybdenum Site of Sulfite Oxidase

M. Jake Pushie,[†] Christian J. Doonan,[†,‡] Heather L. Wilson,[§] K. V. Rajagopalan,[§] and Graham. N. George*[,†]

[†]Geological Sciences, University of Saskatchewan, 114 Science Place, Saskatoon, Saskatchewan S7N 5E2, Canada

[‡]School of Chemistry and Physics, University of Adelaide, Adelaide, South Australia 5005, Australia

[§]School of Medicine, Duke University, Durham, North Carolina 27710, United States

Supporting Information

ABSTRACT: Valuable information on the active sites of molybdenum enzymes has been provided from both Mo^{V} electron paramagnetic resonance (EPR) spectroscopy and X-ray absorption spectroscopy (XAS). One of three major categories of Mo^{V} EPR signals from the molybdenum enzyme sulfite oxidase is the low-pH signal, which forms in the presence of chloride. Two alternative structures for this species have been proposed, one in which the chloride is coordinated directly to Mo and a second in which chloride is held in the arginine-rich basic pocket some 5 Å from Mo. Here we present an independent assessment of the structure of this species by using XAS of the analogous bromide and iodide complexes. We show that there is no evidence of direct Mo−I coordination, and that the data are consistent with a structure in which the halide is bound at ∼5 Å from Mo.

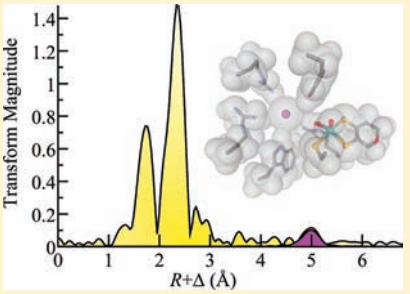

INTRODUCTION

Sulfite oxidase is the physiologically vital oxo-transferase enzyme responsible for oxidation of sulfite to sulfate.[1] Residing in the mitochondrial inner-membrane space, the enzyme is dimeric with a subunit mass of about 52,000. Each monomer contains molybdenum associated with a single pyranopterin dithiolene cofactor,[2] and a cytochrome b_5 heme. The two-electron oxidation of sulfite to sulfate occurs at the Mo site, which is reduced from Mo^{VI} to Mo^{IV} in the process:

$$\text{Enzyme}-Mo^{VI} + SO_3^{2-} + H_2O \rightarrow \text{Enzyme}-Mo^{IV} + SO_4^{2-} + 2H^+$$

The catalytic cycle is completed with reoxidation of the molybdenum first to Mo^{V}, and then to Mo^{VI}, by intramolecular electron transfer to the cytochrome b_5 site, with cytochrome *c* serving as electron acceptor.[3−5]

Sulfite oxidase has been intensively studied by crystallography[6−8] and a variety of spectroscopic methods, including electron paramagnetic resonance (EPR) and X-ray absorption spectroscopy (XAS).[5] The enzyme gives Mo^{V} EPR signals that can be divided into three different categories (Figure 1).[9] The High-pH signal occurs at low anion concentrations and at high pH values,[10,11] while the Low-pH signal occurs at low-pH and at high chloride concentrations.[12] A third category of signals is observed in the presence of oxy-anions and involves coordination of the Mo through one of the oxygens of the oxy-anion. As discussed by Pushie and George,[5] these signals include those from bound inhibitors such as phosphate or arsenate[13−15] as well as sulfite[16] and possibly sulfate.[17−20]

The nature of the Low-pH signal-giving species has been the subject of some debate. Bray and co-workers noted that the signal shows broader line-widths than other sulfite oxidase Mo^{V} EPR signals and attributed this to unresolved hyperfine interaction with $I = {}^3/_2$ ^{35}Cl and ^{37}Cl nuclei and suggested that chloride provided a ligand to molybdenum.[12] Doonan et al.[21] reported that the signal was much sharper in the rigorous absence of chloride, and observed differential broadening of the Mo^{V} EPR signal at both X and S band microwave frequencies with ^{35}Cl and ^{37}Cl.[21] These isotopes both have $I = {}^3/_2$ but with only slightly different g_n values of 0.548 and 0.456, respectively, giving rise to weak hyperfine interactions.[21] From the observed broadening at both X and Q-band microwave frequencies Doonan et al. estimated[35,37]Cl hyperfine couplings of the order of 4 MHz and concluded that the coupling is likely due to a Mo−Cl *trans* to the Mo═O group of the signal-giving species.[21] Coupling to[35,37]Cl was also observed by electron spin echo envelope modulation (ESEEM) by Astashkin et al.,[22] and these workers also concluded that Mo−Cl was likely to be *trans* to the Mo═O of the signal-giving species.[22] Crystallographic studies have observed both sulfate and chloride located in a basic pocket approximately 5 Å from molybdenum, although how this species relates to the EPR signal giving species is not clear.[6,7] The different structures postulated for the signal-giving species are shown in Figure 2. A subsequent pulsed EPR study accurately measured both the hyperfine and the quadrupole couplings of the low-pH chloride signal at about 4.5 and 3 MHz, respectively.[23] These workers employed density functional theory (DFT) to estimate hyperfine and quadrupole couplings for the different structures shown in Figure 2. For directly coordinated chloride the calculated chlorine hyperfine was close to 10 MHz and much larger than the experimental value of 4.5 MHz, whereas for chloride located in the ∼5 Å basic pocket the calculated hyperfine was much smaller

Received: May 16, 2011
Published: September 06, 2011

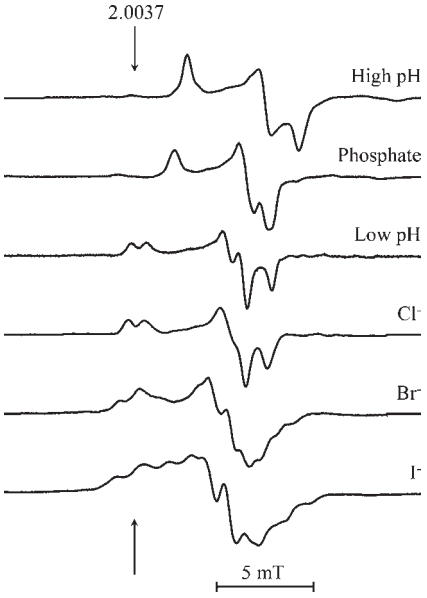

Figure 1. Major Mo^V EPR signals of sulfite oxidase compared with the spectra of the halide complexes. All spectra have been aligned on a common *g*-value scale. The sample for the spectrum indicated as Low pH was prepared under very low chloride conditions, as previously described.[21].

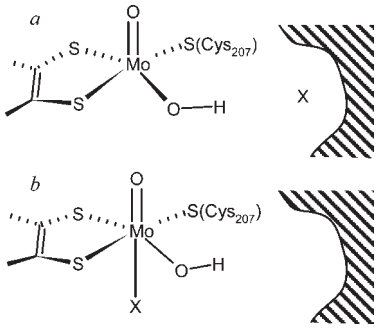

Figure 2. Proposed structures of the Mo^V EPR Low-pH/halide signal-giving species. In (*a*) halide (X^-) is located in an arginine-rich basic pocket (shown shaded) ~5 Å from Mo, in (*b*) the halide is directly coordinated to Mo *trans* to the Mo=O group.

at about 1.5 MHz. The differences for the quadrupole coupling were much larger with calculated values for directly coordinated chloride of more than 19 MHz and about 2 MHz for chloride in the ~5 Å pocket. These workers concluded that the hyperfine coupling was consistent with halide coordination to Mo but that the nuclear electric quadrupole coupling was not.[23] We note that other structural factors such as water or an amino acid residue hydrogen bonding to directly bound chloride might serve to decrease the value of the quadrupole coupling. The combined pulsed EPR and DFT study[23] concluded that Cl^- was *probably not* bound directly to Mo, and was likely to be located in the arginine-rich pocket ~5 Å from the Mo.[6,7,23]

Doonan et al.[21] reported that bromide and iodide gave similar complexes to chloride (Figures 1 and 2). Bromine has two naturally abundant stable magnetic isotopes ^{79}Br and ^{81}Br (50.5 and 49.5% natural abundance, respectively) both with $I = {}^3/_2$ and with similar nuclear *g*-values (1.404 and 1.513, respectively). Iodine has a single stable magnetic isotope ^{127}I with $I = {}^5/_2$ and a nuclear *g*-value of 1.872. If all other factors are equal, both anisotropic and isotropic hyperfine couplings to bromine and iodine are expected to be similar, and about a factor of approximately 4.5 larger than those of chlorine. In agreement with this, all three halide complexes show very similar Mo^V EPR *g*-values and ^1H hyperfine couplings, and the bromide and iodide Mo^V EPR signals showed ~4.5 fold larger halide hyperfine couplings and evidence of significant nuclear quadrupole coupling.[21] It therefore seems very likely that the structures of the Mo^V EPR signal-giving species are analogous, or at least related. X-ray absorption spectroscopy and in particular Extended X-ray Absorption Fine Structure (EXAFS) can provide direct and quantitative information on the coordination of metal ions within complex samples. EXAFS can readily distinguish backscatterers with different numbers of electrons, such as nitrogen and sulfur, but cannot easily distinguish backscatterers with similar numbers of electrons, such as sulfur and chlorine. Thus, a potential chloride ligand would not be distinguishable from the sulfur ligands that are known to be present in the sulfite oxidase Mo site (one cysteinyl sulfur and two from the cofactor dithiolene; Figure 2). Conversely, both bromine and iodine are trivial to distinguish by EXAFS from sulfur, and we present herein a study using Mo K-edge EXAFS of the sulfite oxidase bromide and iodide-bound low-pH species.

MATERIALS AND METHODS

EPR Spectroscopy. Mo^V EPR spectra were recorded on a JEOL RE1X spectrometer at the Stanford Synchrotron Lightsource located near to the beamline used for X-ray absorption spectroscopy measurements. Spectra were recorded at 100 K with 0.1 mT modulation amplitude and were integrated by reference to a Cu^{II}-EDTA standard.

Sample Preparation. Reagents were obtained from Sigma-Aldrich Chemical Co. and were of the best quality available. Samples were prepared in a mixed buffer system consisting of 50 mM bis-tris-propane (1,3-bis(tris(hydroxymethyl)methylamino)propane) and 50 mM MES (2-(*N*-morpholino)ethanesulfonic acid). Purified recombinant human sulfite oxidase was obtained as previously described.[24] Care was taken to exclude chloride from reagents and buffers, essentially following the procedures outlined by Bray and co-workers.[12] In the absence of added chloride the enzyme did not give the typical low-pH chloride signal which has line-broadening arising from unresolved^{35,37}Cl hyperfine structure,[21] and instead gave mixtures of the sharper signal shown in Figure 1 (Low pH) and the high-pH signal. Addition of ~1 mM chloride gave a decrease in the intensity of the high-pH signal and additional amounts of typical broadened low-pH chloride signals that could be discerned by difference spectroscopy (Supporting Information, Figure S1) as reported by Bray and co-workers.[12] From these data and from comparison with those of Bray and co-workers[12] we estimate that residual chloride in our samples is probably below 1 mM. Samples for X-ray absorption spectroscopy (XAS) used concentrated solutions of sulfite oxidase (approximately 0.5 mM Mo) in the presence of either 200 mM NaI or NaBr, and were reduced with 1 mM (final) sodium sulfite solution for approximately 1 min. The resulting reduced enzyme sample was divided into two aliquots, one loaded into an acrylic 1 × 10 × 10 mm^3 XAS cuvette and the other into a quartz 3 mm internal diameter EPR tube. Both samples were then simultaneously frozen by careful immersion in liquid nitrogen, and the Mo^V EPR signal recorded to ensure that the correct species was being investigated.[21]

XAS Data Collection. XAS measurements were conducted at the Stanford Synchrotron Radiation Lightsource (SSRL) with the SPEAR

storage ring containing close to 200 mA at 3.0 GeV. Data were collected using the structural molecular biology XAS beamlines 9−3 and 7−3. Both beamline 9−3 and 7−3 are equipped with a rhodium-coated vertical collimating mirror upstream of the monochromator, and beamline 9−3 has an additional downstream bent-cylindrical focusing mirror (also rhodium-coated). Harmonic rejection was accomplished by setting the cutoff angle of the mirrors to 23 keV. Incident and transmitted X-rays were monitored using argon-filled gas ionization chambers and X-ray absorption was measured as the Mo K_α fluorescence excitation spectrum using an array of 30 germanium detectors.[25] During data acquisition samples were maintained at a temperature of approximately 10 K using an Oxford instruments CF1204 helium cryostat. For each sample between 12 and 8 scans each of approximately 40 min duration were accumulated, and the energy was calibrated by reference to the absorption of a molybdenum foil measured simultaneously with each scan, assuming a lowest energy inflection point of 20003.9 eV.

A significant excess of bromide and iodide is required for quantitative generation of the corresponding halide-bound forms.[21] For the bromide complex the resulting very intense Br K_α fluorescence gave rise to very high count-rates which would have saturated the germanium detector because of electronic dead-time effects.[25] This problem was partially relieved by inserting a neutral filter consisting of a 0.5 mm thick sheet of metallic aluminum positioned between the sample and the detector. The higher energy of the Mo K_α relative to the Br K_α (17.4 keV vs11.9 keV) means the former will be less attenuated by a neutral filter. Thus, 0.5 mm of aluminum will absorb approximately 50% of the Mo K_α and approximately 85% of the Br K_α. The neutral filter was used in combination with a zirconium filter which was used to preferentially absorb scattered radiation, together with silver Soller slits positioned so as to preferentially accept photons coming directly from the sample and reject filter fluorescence. These precautions allowed XAS data to be collected for the bromide complex, although the signal-to-noise of precluded data collection beyond $k = 14$ Å^{-1}. For the iodide complex, the much lower energies of the iodine L-edge X-ray fluorescence (ca. 3.9−4.2 keV) meant that this was essentially totally absorbed by the zirconium filter and by the window materials in the cryostat and the detector, so an additional neutral filter was not required. In this case the data collection extended to $k = 17$ Å^{-1}.

XAS Data Analysis. The EXAFS oscillations $\chi(k)$ were quantitatively analyzed by curve-fitting using the EXAFSPAK suite of computer programs,[26] as described by George et al.,[27] using ab initio theoretical phase and amplitude functions calculated using the program FEFF version 8.25.[28] The threshold energy ($k = 0$ Å^{-1}) of the EXAFS oscillations was assumed to be 20025.0 eV.

Density Functional Theory. Density Functional Theory (DFT) calculations employed the programs Dmol^3 Materials Studio Version 5.5.[29,30] Geometry optimization calculations used Becke exchange[31] and Perdew correlation[32] functionals for both the potential during the self-consistent field procedure and the energy. Dmol^3 uses numerically derived basis sets,[29,30] and these included polarization functions for all atoms. Calculations were spin-unrestricted and all-electron core potentials were used. Solvation effects were modeled using the Conductor-like Screening Model (COSMO)[33] in Dmol^3 with a dielectric value representing water ($\varepsilon = 78.39$). Convergence was said to be achieved when energies differed by less than 2×10^{-5} Hartree, the maximum force was less than 0.004 hartree/Å, and the maximum displacement was less than 0.005 Å. A maximum step size of 0.3 Å was used. Calculation of spin densities used the same conditions as the geometry optimizations, except that the more rigorous Perdew−Burke−Ernzerhof functional was used,[34,35] with an all-electron relativistic core treatment.

Molecular Dynamics. Molecular Dynamics (MD) simulations were carried out using GROMACS version 3.3.3[36,37] as previously described.[38] The all-atom OPLS-AA/L force field[39,40] was employed for simulations, supplemented by parameters for the Mo and Fe coordinating environments, detailed previously.[38] The temperature was kept constant (300 K, $\tau_T = 0.1$ ps) by weakly coupling the system to an external temperature bath.[41] Interactions were updated iteratively using a grid-based neighbor search algorithm and was updated every 10 steps with a neighbor list of 1 nm. Pressure was maintained at 1 bar with isotropic temperature coupling ($\tau_P = 1.0$ ps) and compressibility of 4.5×10^{-5} bar^{-1}. The Particle-Mesh Ewald (PME) method was employed for long-range electrostatics, with a cutoff of 1 nm.[42] The linear constraint solver (LINCS) was used to constrain bond lengths within the protein and prosthetic groups.[43] The van der Waals interactions were calculated using a cutoff of 1 nm. Simple point charge (SPC) waters were used in all simulations and were constrained using SETTLE.[44]

To make the simulations more computationally tractable, we elected to employ a longer time step per iteration to reach longer durations. The most direct way this can be achieved is to slow the fastest motions within the simulation, that is, R—H bond vibrations. To this end the mass of all hydrogen atoms was increased to 4.032 mu, and the increased mass was concomitantly subtracted from their parent heavy atoms to maintain the same total mass of the system. Within the protein this effectively reduces the vibrational frequency of C/O/N−H bonds and slows dihedral motions. With such changes, a longer 5 fs time step was implemented, as has been successfully demonstrated previously.[43,45−47] This time step was chosen as a small but reasonable increase above the more commonly implemented 2 fs time step used in GROMACS simulations. Inappropriately long time steps can cause energy instabilities in the simulations leading to heating because of force errors which would be reflected in the results.[48] We therefore monitored the temperature and λ (a measure of heat flow between the simulation and the external bath) for each simulation. Temperatures averaged from all simulation data were 299.659 ± 0.001 with an rmsd of 0.868 ± 0.002 and a total drift (over the entire simulation times) was 0.000 ± 0.053, while λ for the protein and nonprotein systems averaged to 1 in all cases, indicating no significant heating or cooling effect from the external bath.

Starting coordinates for the protein used a representative structure from a previous MD simulation of the half-dimer.[38] The half-dimer was simulated in a square box, 85 Å per side, with periodic boundary conditions. The box was filled with 17616 SPC water molecules, 1 I^- and 11 Na^+ counterions, for a total system charge of zero. The I^- atoms were manually inserted into the active site channel at positions approximately the same as those occupied by sulfate in the 1SOX crystal structure, with the expectation that these would be sufficiently close as to allow the iodide atoms to explore the local environment within the active site channel and reach a preferred locale during the simulations.[6] The topology for the iron-bound heme as well as the molybdenum-containing active site have been previously described.[38] The system was energy minimized and then 12 simulations were separately equilibrated for 5 ns prior to production runs (protein root-mean square deviations stabilized in all simulations by ∼2 ns). Each of the 8 simulations were run uncoupled to one another, in parallel, for 55−65 ns each (total simulation time = ∼0.72 ms).

RESULTS AND DISCUSSION

Figures 3 and 4 show the EXAFS Fourier transform of the bromide and iodide complexes. Both EXAFS spectra show two major peaks in their Fourier transforms, which arise from Mo═O and Mo−S backscattering (Figures 3, 4) with a smaller contribution from Mo−O that is partly hidden by the intense Mo−S EXAFS.[5] The spectra are typical of reduced forms of sulfite oxidase (either Mo^V or Mo^{IV}) which shows a weaker Mo═O peak because of the presence of only a single such ligand, compared to two in the oxidized enzyme.[5,49] Double integration of the Mo^V EPR signals indicated that like the chloride complex[9,12] the samples were approximately 35% Mo^V, and are

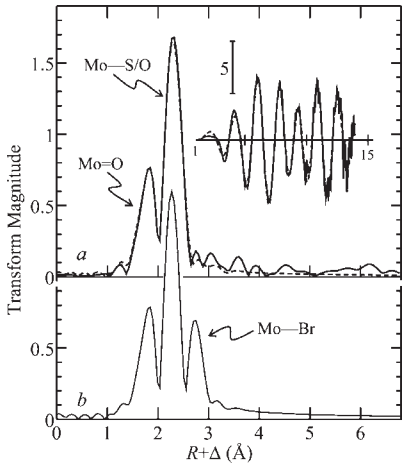

Figure 3. EXAFS Fourier transform of sulfite oxidase Low-pH bromide complex phase-corrected for Mo−S backscattering. (*a*) shows the experimental data (solid line) together with the best fit (broken line). The inset shows the k^3-weighted EXAFS oscillations plotted against k (range 1−14 Å^{-1}). (*b*) shows a simulated EXAFS Fourier transform for direct Mo−Br coordination assuming a bond-length of 2.67 Å (obtained from DFT calculations of Figure 2b). Table 1 gives the structural parameters derived from EXAFS curve-fitting.

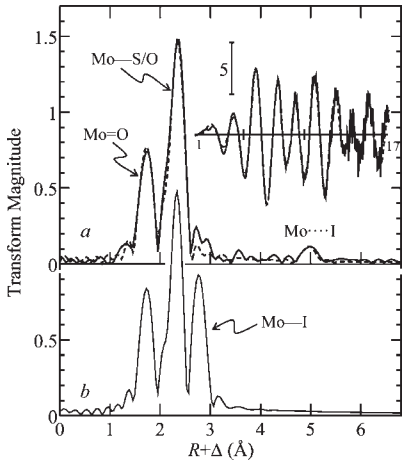

Figure 4. EXAFS Fourier transform of sulfite oxidase Low-pH iodide complex phase-corrected for Mo−S backscattering. (*a*) shows the experimental data (solid line) together with the best fit (broken line). The inset shows the k^3-weighted EXAFS oscillations plotted against k (range 1−17 Å^{-1}). (*b*) shows a simulated EXAFS Fourier transform for direct Mo−I coordination assuming a bond-length of 2.75 Å (obtained from DFT calculations of Figure 2b). Table 1 gives the structural parameters derived from EXAFS curve-fitting. The putative long-range Mo····I interaction is identified in (*a*).

expected to be a mixture of Mo^V and Mo^{IV} oxidation states.[9,12] The Mo K near-edge spectra of the bromide and iodide complex were shifted to lower energy relative to the spectrum of fully oxidized enzyme (Figure 5), which is consistent with a mixture of reduced forms for these samples. The EXAFS will therefore provide averaged structural information for Mo^V and Mo^{IV}. We note in passing that the corresponding spectrum for the chloride complex is qualitatively similar;[50] although the available data have lower energy resolution so the features of the near-edge spectra are broadened relative to those of Figure 5. Our goal in

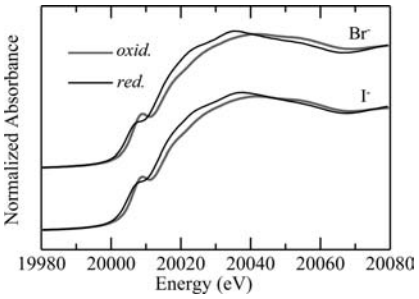

Figure 5. Molybdenum K near-edge spectra of sulfite oxidase bromide and iodide complexes (labeled *red.*) compared with that of oxidized enzyme (labeled *oxid.*). The spectra of the halide complexes can be seen to be very similar to each other and shifted to lower energy relative to the spectrum of oxidized enzyme, confirming the presence of a reduced active site.

these experiments was to unambiguously determine which of the two alternative postulated structures shown in Figure 2 occurred in the enzyme active site.

Quantitative fitting of the EXAFS spectra of the bromide and iodide samples indicated very similar active sites. Both were quantitatively fitted with a single Mo=O at 1.71 Å, three Mo−S at ∼2.39 Å, and one Mo−O at ∼2.06 Å. Figures 3 and 4 also shows simulations of the EXAFS Fourier transform that would be expected if direct Mo−I or Mo−Br coordination were present. The simulations used Mo—X bond-lengths obtained from DFT energy optimized geometries,[21] of 2.67 and 2.75 Å for Mo−Br and Mo−I, respectively. The simulations illustrate that intense bromine and iodine EXAFS backscattering would be observed with these directly coordinated halide ligands, particularly for the iodide complex. The fact that no such intense EXAFS is observed clearly indicates the lack of direct bromide and iodide coordination to molybdenum, and by implication that the chloride complex does not possess Mo−Cl coordination. The experimental EXAFS Fourier transform of the iodide sample does show a small peak at ∼2.9 Å, which is close to the expected location of a Mo−I interaction. This can be partly fitted by ∼0.1 iodine atoms with a large Debye−Waller factor, but the overall fit is not markedly improved, and we conclude that this does not provide credible evidence for Mo−I bonding.

The experimental Fourier EXAFS transform of the iodide sample also shows a small long-distance peak at approximately 5 Å. Neglecting the effects of the Debye−Waller and electron mean-free path terms,[5] EXAFS amplitude scales approximately as the inverse square of the interatomic distance. Observation of distant backscatterers is thus highly unusual in EXAFS spectroscopy, especially when no direct covalent path is present, and it is common practice to ignore such small peaks. Nevertheless, we observed that the interatomic distance is very close to that expected for the proposed binding site to the arginine-rich pocket that we have discussed above (Figure 2).[6,23] Moreover, this small transform peak is above the noise level, it persists when the Fourier transform was computed using different k-ranges, and it diminishes in amplitude when phase-correction is removed. Noise peaks frequently diminish or disappear when different k-ranges are used and become relatively more intense when phase-correction is not applied. The ∼5 Å peak thus appears as to be a bona fide EXAFS interaction, and we therefore attempted curve-fitting analysis which showed that the feature fitted well to a Mo····I interaction at 4.99 Å. The other possible identity for the ∼5 Å peak are the two distant carbons coordinated to the ditholene carbons in the cofactor pyran ring,

dx.doi.org/10.1021/ic201030u |*Inorg. Chem.* 2011, 50, 9406–9413

which are expected to be at about 4.85 Å from Mo. EXAFS simulations (not illustrated) required physically impossible (negative) Debye−Waller factors to obtain the observed ∼5 Å intensity, and we therefore discarded this possibility. Thus, the putative Mo····I interaction is above the noise level, behaves as if the iodine is backscattering the outgoing photoelectron, and is at the distance expected for halide binding in the basic pocket bounded by three arginine residues. We therefore tentatively assign this feature to the iodide observed through its hyperfine interaction with the Mo^V with EPR spectroscopy. As noted above, the sample is a mixture of Mo^{IV} and Mo^V formal oxidation states, and if the tentative assignment of a ∼5 Å Mo····I interaction is correct then iodide would be expected to be similarly located in both oxidation states. We note in passing that most sulfite oxidase crystal structures are derived from samples that were initially oxidized Mo^{VI} and photoreduced during data acquisition to Mo^V and Mo^{IV}, changing with time and exposure, and correspond to a structure of predominantly reduced forms, probably a mixture of Mo^V and Mo^{IV}.[6,7] In this case the sulfate observed in the ∼5 Å active site pocket does not appear disordered.

The ionic radius of iodide at around 2.20 Å is significantly larger than chloride or bromide (1.81 and 1.96 Å, respectively) and the conformational flexibility of the basic pocket might be restricted by the larger iodide when compared to the other halides, which might in turn reduce the Debye−Waller factor and help explain its unexpected observation by EXAFS. Moreover, the proton of the Mo−OH group, which gives rise to the hyperfine coupling observed in the low-pH signal, might further stabilize the complex by hydrogen bonding to the anion. Neglecting the effects of charge, that the active site pocket ∼5 Å from molybdenum can accommodate iodide is clear experimentally from crystallographic data showing sulfate in the pocket,[6] as sulfate has about the same molecular volume as the iodide ion. We further explored the feasibility of iodide binding to sulfite oxidase using both DFT and MD calculations.

DFT calculations included six active site amino acids: Try343, Trp226, Arg160, Arg190, Arg472, and Cys207 which is coordinated to molybdenum. The pyran ring of the cofactor was included, and pendant bonds were terminated with hydrogens. The calculations employed geometric constraints from the crystal structure. The alpha carbons of the amino acids and the pyran ring carbons were constrained to their crystallographic positions, as were the vectors described by the alpha and beta carbons.[21] The energy minimized structures show that any of chloride, iodide, and sulfate are well accommodated in the arginine-rich pocket, as expected from crystal structure data.[6,7] No large scale differences were predicted between Mo^V and Mo^{IV} oxidation states with respect to the disposition of the halide, and the Mo−OH is correctly oriented for hydrogen bonding with the anion as previously suggested.[23] For the Mo^{IV} form a Mo−OH_2 coordination was postulated with the additional proton hydrogen bonding to N_ε of Arg160. The Mo····I distances were found to be 5.25 and 5.31 Å for Mo^V and Mo^{IV}, respectively. Other possible locations of the iodide were tested, such as *trans* to the Mo═O group and ∼5 Å from Mo. These calculations did not converge within 150 iterations because of large motions of the iodide within the overall structure, suggesting that the iodide would in this case not be stably bound. For the Mo^V form with the iodide located in the ∼5 Å pocket, examination of the computed spin density indicated appreciable electron spin on active site atoms, including the Mo−OH group (Figure 6), consistent with the observed and calculated ^1H and ^{17}O and hyperfine splittings from this group.[23]

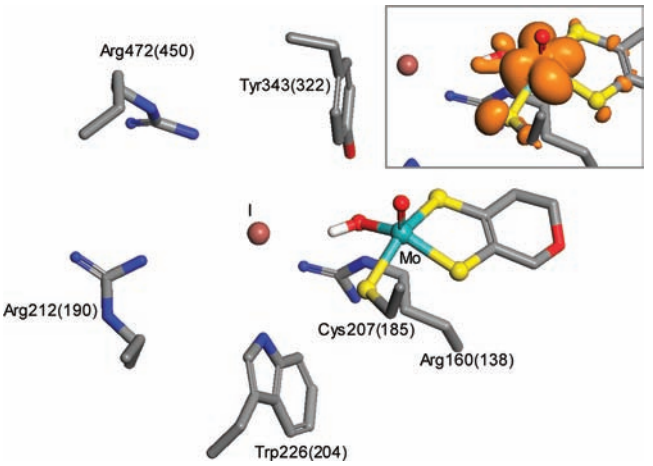

Figure 6. DFT energy minimized structure showing iodide within the anion binding pocket ∼5 Å from molybdenum for the Mo^V form of the enzyme bearing a Mo−OH group. The inset shows the spin density isosurface with a value of 0.013 electrons per cubic a.u. showing spin localization on various active site atoms including the Mo−OH group.

The sulfite oxidase crystal structures identify two anion binding pockets within the channel leading to the Mo active site.[6,7] The first binding site is that at 5.2 Å from Mo and which we have already discussed. It lies in a basic pocket bounded by three arginine residues, and crystal structures with sulfate[6] or chloride[7] in this pocket have been reported. The second site is approximately 10−11 Å distant from Mo, at the entrance to the channel leading to the active site, close to the surface of the protein. Iodide bound in either the 5 or 11 Å pocket are shown in Figure 7. This site has been observed by crystallography to contain sulfate[6] but not chloride in sulfate-free conditions.[7] During the course of the MD simulations the iodide atom, which starts within the active site channel in the vicinity of the 5 Å or 11 Å pocket, explores multiple stable interaction sites. The majority of stable binding pockets lie at approximately 5 and 10 Å from the molybdenum center. Multiple and different transiently stable binding pockets were sampled during the simulations at approximately 5.5, 6, 7.5, 8, 9.5, and 11 Å from the molybdenum center; however, these were typically only occupied for <5 ns during the course of any given simulation before the iodide found one of the more stabilizing 5 or 10 Å sites, or exited the active site channel altogether. The most stable iodide interaction site from all of the simulations was at 5.2 ± 0.3 Å from the molybdenum, with an interaction energy of −203 ± 15 kJ mol^{-1} between iodide and the surrounding environment (including protein residues, the molybdenum-bound prosthetic group and solvent occupying the active side channel). The bulk of the interaction energy in the 5.2 Å pocket, contributing −118 ± 15 kJ mol^{-1}, is composed of interactions with specific water molecules which are in a H-bond network in the active site pocket and the surrounding channel. The strongly stabilizing interaction between iodide and its local environment can be compared with the interaction energy of iodide and bulk solvent from simulations where the iodide has exited the active site, which is −194 ± 21 kJ mol^{-1} (average from all relevant simulation data). A summary of interaction energies for iodide, at various stable distances from the molybdenum center within the active site channel, are contained in the Supporting Information, Table S1. In most simulations the iodide was only retained in the active site channel for 25−50 ns.

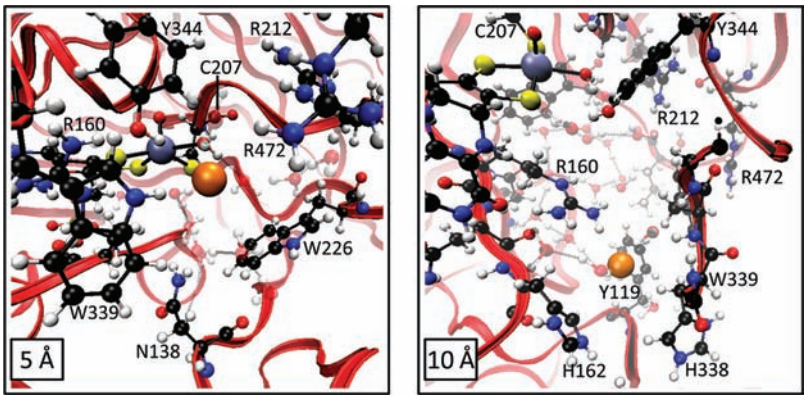

Figure 7. Representative MD simulation snapshots where I^- occupies positions at 5.2 ± 0.3 Å and 11.2 ± 0.4 Å, respectively. Rendering of solvent molecules within the active site channels has been de-emphasized to enhance the local protein structure in the anion binding pockets.

The simulation where the iodide was in the most stabilizing binding pocket (at 5.2 ± 0.3 Å) was the only simulation that retained the iodide for the duration of the simulation. In two of the simulations (one each from the simulations initiated with iodide at 5 and 10 Å from the molybdenum active site) the iodide re-entered the channel ~30 ns after its exit, while in the interim the Mo····I distance was as much as 68 Å. The interactions energies between iodide and the residues at the opening of the active site channel are approximately the same as those observed when iodide occupies the 10−11 Å binding pocket. During the initial capture event, residues Asn138, Arg160, and His162 showed the strongest interactions with the anion. Although these simulations used a monoanionic counterion and demonstrate the stability of the anion binding pockets within the active site channel, the initial capture of a dianionic species, such as SO_3^{2-}, would be significantly stronger and is likely to recruit additional nearby residues to aid charge compensation. Although similar in radius to iodide, SO_3^{2-} is also likely to organize its surrounding environment with a subtly different H-bonding network from iodide.

On the basis of the MD simulation data, we also note that when the iodide occupies the 5.2 Å binding pocket its interaction energy with the surrounding environment is less variable, compared to when it is located in the 10−11 Å pocket or at intermediate distances; furthermore, the atom is held much more rigidly, as evidenced from the small variability in its position from the Mo center. This stability in iodide position lends support to our assertion that in the 5.2 Å pocket iodide serves as a good back-scattering atom at this unusually long distance from the Mo center.

Our results unequivocally show that the sulfite oxidase Low-pH iodide and bromide complexes do not contain a halide ligand to Mo, and support a structure for the signal-giving species in which the iodide is contained within the arginine-rich basic pocket adjacent to Mo.[23] The halide-free Mo^V EPR signal-giving species reported by Doonan et al.[21] probably has either a bisulfite, sulfite, or sulfate in the arginine-rich basic pocket, with hydrogen bonding to the Mo−OH group as postulated for the halide complexes. Of these possibilities we favor bisulfite $[HSO_3]^-$, which has a similar radius to iodide, because like the halides it is a monoanion, and hence the resulting EPR signal might be expected to be similar to those from halides. Moreover, the signal forms preferentially at pH values lower than the second pK_a of sulfite ($HSO_3^- \leftrightarrow H^+ + SO_3^{2-} \sim 7$ in water) which would also favor a bisulfite complex.

Table 1. Mo K-Edge EXAFS Curve-Fitting Results[a]

species	interaction	N	R	σ^2	ΔE_0
iodide [b]	Mo═O	1	1.711(1)	0.0014(2)	−12.8(8)
	Mo−S	3	2.391(2)	0.0033(1)	
	Mo−O	1	2.06(3)	0.007(5)	
	Mo····I	1	4.99(1)	0.0057(8)	
bromide [c]	Mo═O	1	1.710(3)	0.0016(2)	−13.8(7)
	Mo−S	3	2.375(3)	0.0030(1)	
	Mo−O	1	2.03(1)	0.006(1)	

[a] Coordination numbers, N, interatomic distances R (Å), Debye−Waller factors σ^2 (Å^2), and threshold energy shift ΔE_0 (eV). Values in parentheses are the estimated standard deviations obtained from the diagonal elements of the covariance matrix. [b] Data were fitted between $k = 1$ and 17 Å^{-1}. [c] Data were fitted between $k = 1$ and 14 Å^{-1}. Inclusion of Mo−Br interactions did not improve the quality of the fits.

The presence of hyperfine coupling to nearby magnetic nuclei has often been taken as definitive evidence for coordination of the group containing the magnetic nucleus. Thus, in *Escherichia coli* nitrate reductase Mo^V effects of halides and in particular hyperfine coupling to ^{19}F in the fluoride complex have been taken as evidence of Mo−F coordination.[51] There now seems reason to doubt that the halide is actually coordinated to Mo in nitrate reductase, and a remote association resembling that discussed here for sulfite oxidase[23] seems more likely.

In early work, Bray and co-workers investigated the suggestion that low levels of chloride might be important for the enzyme to attain full catalytic activity.[12] Bray and co-workers confirmed earlier observations of significant inhibition of sulfite oxidase in the presence of high levels of chloride[52] and concluded that there was no evidence for a requirement for chloride by sulfite oxidase.[12] Later work confirmed that chloride inhibits with a K_I of approximately 4 mM,[53] and subsequent comprehensive studies of sulfite oxidase kinetics have excluded chloride for this reason. It now seems clear that the mechanism of inhibition by chloride, and probably by bromide and iodide, is to block the active site anion binding pockets adjacent to molybdenum, rather than any role which involves direct coordination of molybdenum. Indeed, our MD simulations suggest that halide ions can associate with both the near pocket, ~5 Å from Mo, and the more distant one, at ~11 Å from Mo, thereby providing two sites for inhibitory binding.

dx.doi.org/10.1021/ic201030u |*Inorg. Chem.* 2011, 50, 9406–9413

■ ASSOCIATED CONTENT

Supporting Information. Further details are given in Figure S1 and Tables S1 and S2. This material is available free of charge via the Internet at http://pubs.acs.org.

■ AUTHOR INFORMATION

Corresponding Author
*E-mail: g.george@usask.ca.

■ ACKNOWLEDGMENT

Work at the University of Saskatchewan was supported by the Natural Sciences and Engineering Research Council, a Canada Research Chair award (G.N.G.), the University of Saskatchewan and the Canadian Institutes for Health Research (CIHR). Postdoctoral fellowships from the Saskatchewan Health Research Foundation, CIHR and CIHR-THRUST (M.J.P.). Work at Duke University was supported by National Institute of Health (NIH) Grant GM00091 (K.V.R.). Portions of this work were carried out at the Stanford Synchrotron Radiation Lightsource which is funded by the U.S. DOE, Office of Basic Energy Sciences and Office of Biological and Environmental Sciences, and the National Institutes of Health, National Center for Research Resources.

■ REFERENCES

(1) McLeod, R. M.; Farkas, W.; Fridovitch, I.; Handler, P. *J. Biol. Chem.* **1961**, *236*, 1841–1852.
(2) (a) Rajagopalan, K. V. *Adv. Enzymol. Relat. Areas Mol. Biol.* **1991**, *64*, 215–290. (b) Rajagopalan, K. V.; Johnson, J. L. *J. Biol. Chem.* **1992**, *267*, 10199–10202.
(3) Cohen, H. L.; Betcher-Lange, S.; Kessler, D. L.; Rajagopalan, K. V. *J. Biol. Chem.* **1972**, *247*, 7759–7766.
(4) Johnson, J. L.; Rajagopalan, K. V. *J. Biol. Chem.* **1977**, *252*, 2017–2025.
(5) Pushie, M. J.; George, G. N. *Coord. Chem. Rev.* **2011**, *255*, 1044–1084.
(6) Kisker, C.; Schindelin, H.; Pacheco, A.; Wehbi, W. A.; Garrett, R. M.; Rajagopalan, K. V.; Enemark, J. E.; Rees, D. C. *Cell* **1997**, *91*, 1–20.
(7) Karakas, E.; Wilson, H. L.; Graf, T .N.; Xiang, S.; Jaramillo-Busquets, S.; Rajagopalan, K. V.; Kisker, C. *J. Biol. Chem.* **2005**, *280*, 33506–33515.
(8) Qiu, J. A.; Wilson, H. L.; Pushie, M. J.; Kisker, C.; George, G. N.; Rajagopalan, K. V. *Biochemistry* **2010**, *49*, 3989–4000.
(9) Lamy, M. T.; Gutteridge, S.; Bray, R. C. *Biochem. J.* **1980**, *185*, 397–403.
(10) George, G. N. *J. Magn. Reson.* **1985**, *64*, 384–394.
(11) Astashkin, A. V.; Mader, M. L.; Pacheco, A.; Enemark, J. H.; Raitsimring, A. M. *J. Am. Chem. Soc.* **2000**, *122*, 5294–5302.
(12) Bray, R. C.; Gutteridge, S.; Lamy, M. T.; Wilkinson, T. *Biochem. J.* **1983**, *211*, 227–236.
(13) George, G. N.; Prince, R. C.; Kipke, C. A.; Sunde., R. A.; Enemark, J. E. *Biochem. J.* **1988**, *256*, 307–309.
(14) Pacheco, A.; Basu, P.; Borbat, P.; Raitsimring, A. M.; Enemark, J. H. *Inorg. Chem.* **1996**, *35*, 7001–7008.
(15) George, G. N.; Garrett, R. M.; Graf, T.; Prince, R. C.; Rajagopalan, K. V. *J. Am. Chem. Soc.* **1998**, *120*, 4522–4523.
(16) Bray, R. C.; Lamy, M. T.; Gutteridge, S.; Wilkinson, T. *Biochem. J.* **1982**, *201*, 241–243.
(17) Astashkin, A. V.; Hood, B. L.; Feng, C.; Hille, R.; Mendel, R. R.; Raitsimring, A. M.; Enemark, J. H. *Biochemistry* **2005**, *44*, 13274–13281.
(18) Astashkin, A. V.; Johnson-Winters, K.; Klein, E. L.; Byrne, R. S.; Hille, R.; Raitsimring, A. M.; Enemark, J. H. *J. Am. Chem. Soc.* **2005**, *128*, 14800–14810.
(19) Astashkin, A. V.; Johnson-Winters, K.; Klein, E. L.; Feng, C.; Wilson, H. L.; Rajagopalan, K. V.; Raitsimring, A. M.; Enemark, J. H. *J. Am. Chem. Soc.* **2008**, *130*, 8471–8480.
(20) Rajapakshe, A.; Johnson-Winters, K.; Nordstrom, A. R.; Meyers, K. T.; Emesh, S.; Atashkin, A. V.; Enemark, J. H. *Biochemistry* **2010**, *49*, 5154–5159.
(21) Doonan, C. J.; Wilson, H. L.; Bennett, B.; Prince, R. C.; Rajagopalan, K. V.; George, G. N. *Inorg. Chem.* **2008**, *47*, 2033–2038.
(22) Astashkin, A. V.; Klein, E. L.; Enemark, J. H. *J. Inorg. Biochem.* **2007**, *101*, 1623–1629.
(23) Klein, E. L.; Astashkin, A. V.; Ganyushin, D.; Riplinger, C.; Johnson-Winters, K.; Neese, F.; Enemark, J. H. *Inorg. Chem.* **2009**, *48*, 4743–4752.
(24) Temple, C. A.; Graf, T. N.; Rajagopalan, K. V. *Arch. Biochem. Biophys.* **2000**, *383*, 281–287.
(25) Cramer, S. P.; Tench, O.; Yocum, M.; George, G. N. *Nucl. Instrum. Meth.* **1988**, *A266*, 586–591.
(26) http://ssrl.slac.stanford.edu/exafspak.html.
(27) George, G. N.; Garrett, R. M.; Prince, R. C.; Rajagopalan, K. V. *J. Am. Chem. Soc.* **1996**, *118*, 8588–8592.
(28) Rehr, J. J.; Mustre de Leon, J.; Zabinsky, S. I.; Albers, R. C. *J. Am. Chem. Soc.* **1991**, *113*, 5135–5140.
(29) Delley, B. *J. Chem. Phys.* **1990**, *92*, 508–517.
(30) Delley, B. *J. Chem. Phys.* **2000**, *113*, 7756–7764.
(31) Becke, A. D. *J. Chem. Phys.* **1988**, *88*, 2547–2553.
(32) Perdew, J. P.; Wang, Y. *Phys. Rev. B* **1992**, *45*, 13244–13249.
(33) Klamt, A.; Schüürmann, G. *J. Chem. Soc. Perkin. Trans* **1993**, *2*, 799–805.
(34) Perdew, J. P.; Burke, K.; Ernzerhof, M. *Phys. Rev. Lett.* **1996**, *77*, 3865–3868.
(35) Perdew, J. P.; Burke, K.; Ernzerhof, M. *Phys. Rev. Lett.* **1997**, *78*, 1396.
(36) Berendsen, H. J. C.; van der Spoel, D.; van Drunen, R. *Comput. Phys. Commun.* **1995**, *91*, 43–56.
(37) Lindahl, E.; Hess, B.; van der Spoel, D. *J. Mol. Model.* **2001**, *7*, 306–317.
(38) Pushie, M. J.; George, G. N. *J. Phys. Chem. B* **2010**, *114*, 3266–3275.
(39) Kaminski, G.; Duffy, E. M.; Matsui, T.; Jorgensen, W. L. *J. Phys. Chem.* **1994**, *98*, 13077–13082.
(40) Jorgensen, W. L.; Maxwell, D. S.; Tirado-Rives, J. *J. Am. Chem. Soc.* **1996**, *118*, 11225–11236.
(41) Berendsen, H. J. C.; Postma, J. P. M.; DiNola, A.; Haak, J. R. *J. Chem. Phys.* **1984**, *81*, 3684–3690.
(42) Essman, U.; Perela, L.; Berkowitz, M. L.; Darden, T.; Lee, H.; Pedersen, L. G. *J. Chem. Phys.* **1995**, *103*, 8577–8592.
(43) Hess, B.; Bekker, H.; Berendsen, H. J. C.; Fraaije, J. G. E. M. *J. Comput. Chem.* **1997**, *18*, 1463–1472.
(44) Miyamoto, S.; Kollman, P. A. *J. Comput. Chem.* **1992**, *13*, 952–962.
(45) Feenstra, K. A.; Hess, B.; Berendsen, H. J. C. *J. Comput. Chem.* **1999**, *20*, 786–798.
(46) Aliste, M. P.; Tieleman, D. P. *BMC Biochem.* **2005**, *6*, 30.
(47) Chan, D. I.; Stockner, T.; Tieleman, D. P.; Vogel, H. J. *J. Biol. Chem.* **2008**, *283*, 33620–33629.
(48) Apol, E.; Apostolov, R.; Berendsen, H. J. C.; van Buuren, A.; Bjelkmar, P.; van Drunen, R.; Feenstra, A.; Groenhof, G.; Kasson, P.; Larsson, P.; Meulenhoff, P.; Murtola, T.; Páll, S.; Pronk, S.; Schulz, R.; Shirts, M.; Sijbers, A.; Tieleman, P.; Hess, B.; van der Spoel, D.; Lindahl, E. *Gromacs User Manual 4.5.4*; Department of Biophysical Chemistry, University of Groningen: Groningen, The Netherlands, 2010; www.gromacs.org.
(49) Harris, H. H.; George, G. N.; Rajagopalan, K. V. *Inorg. Chem.* **2006**, *45*, 493–495.

(50) George, G. N.; Kipke, C. A.; Prince, R. C.; Sunde, R. A.; Enemark, J. H.; Cramer, S. P. *Biochemistry* **1989**, *28*, 5075–5080.
(51) George, G. N.; Bray, R. C.; Morpeth, F. F.; Boxer, D. H. *Biochem. J.* **1985**, *227*, 925–931.
(52) Kessler, D. L.; Rajagopalan, K. V. *Biochim. Biophys. Acta* **1974**, *370*, 389–398.
(53) Sullivan, E. P., Jr.; Hazzard, J. T.; Tollin, G.; Enemark, J. H. *J. Am. Chem. Soc.* **1992**, *114*, 9662–9663.
(54) Brody, M. S.; Hille, R. *Biochemistry* **1999**, *38*, 6668–6677.